FRONTIERS OF PHYSICS

RESEARCH ARTICLE
Volume 18 / Issue 3 / 31303 / 2023

Quantum dynamics studies on the non-adiabatic effects of H + LiD reaction

Yuwen Bai, Zijiang Yang, Bayaer Buren, Ye Mao, Maodu Chen†

Key Laboratory of Materials Modification by Laser, Electron, and Ion Beams (Ministry of Education), School of Physics, Dalian University of Technology, Dalian 116024, China
Corresponding author. E-mail: †mdchen@dlut.edu.cn
Received October 20, 2022; accepted November 30, 2022

ABSTRACT

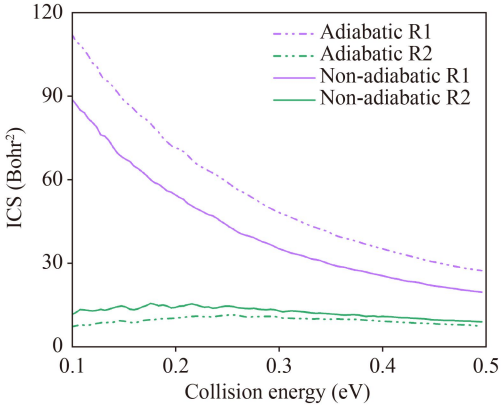

After the Big Bang, chemical reactions of hydrogen with LiH and its isotopic variants played an important role in the late stage of recombination. Moreover, these reactions have attracted the attention of experts in the field of molecular dynamics because of its simple structure. Electronically non-adiabatic effects play a key role in many chemical reactions, while the related studies in LiH_2 reactive system and its isotopic variants are not enough, so the microscopic mechanism of this system has not been fully explored. In this work, the microscopic mechanism of H + LiD reaction are performed by comparing both the adiabatic and non-adiabatic results to study the non-adiabatic effects. The reactivity of R1 (H + LiD → Li + HD) channel is inhibited, while that of R2 (H + LiD → D + LiH) channel is enhanced when the non-adiabatic couplings are considered. For R1 channel, a direct stripping process dominates this channel and the main reaction mechanism is not influenced by the non-adiabatic effects. For R2 channel, at relatively low collision energy, the dominance changes from a rebound process to the complex-forming mechanism when the non-adiabatic effects are considered, whereas the rebound collision approach still dominates the reaction at relatively high collision energy in both calculations. The presented results provide a basis for further detailed study on this importantly astrophysical reaction system.

Keywords non-adiabatic effects, quantum dynamics, time-dependent wave packet, astrophysical reaction

1 Introduction

After the Big Bang, there is no survived atom because any atom would be ionized under this strong background radiation [1]. With the universe cooling, electrons can attach to protons, marking the recombine era beginning [2]. In the early stage of recombine era, there were only some simply atomic nuclei such as H, D, ^{3}He, ^{4}He and ^{7}Li. Due to the characteristics of each element, recombination did not occur simultaneously among these elements. The first element to recombine is helium, and the next element is hydrogen, then lithium element starts to react. In this stage, the reactions are simple, usually binding between ions. As the temperature decreases, chemical reactions gradually occur, such as LiH + He, LiH + H and their isotopic reactions.

The chemical reactions including Li and H elements have been studied for decades due to their importance in astronomy. The reaction results can be revealed by quantum dynamics [3–6], and there are many researches on the quantum dynamics of LiH_2 reaction system. In 1984, Lepp *et al.* [7] calculated the formation of molecules in the postrecombination epoch through gas-phase reactions, including LiH. They proposed that the dipole rotational transitions of LiH and HD must be taken seriously at high density and low temperature. In 1998, Clarke *et al.* [8] studied the depletion and formation

Higher Education Press

https://doi.org/10.1007/s11467-022-1239-1

reactions of LiH molecule related with the universe changing for the first time. They constructed a reaction surface of the two-dimensional collinear process and studied the characteristics of two reactions based on this surface. In 2002, Padmanaban with his coworker [9] reported the reaction probabilities in both collinear and the three-dimensional arrangements of H + LiH system. The research results showed that the reactions prefer to follow a resonance formation path at low energies and a direct path at high energies. In 2012, Roy *et al.* [10] carried out a study of quantum dynamics of H + LiH reaction and its isotopic variants using the time-dependent quantum wave packet (TDWP) method. They also investigated the influence of vibrational excitation of LiH on the reactivity of reaction channels, and found that the vibrational excitation of reagent molecule decreases and increases the reactivity of LiH-depletion and H-exchange channel, respectively. In 2019, Huran *et al.* [11] studied the stereodynamics of H + LiH ($\nu = 0$, $j = 0 - 1$) by analysis the $\boldsymbol{k}$–$\boldsymbol{j}$ and $\boldsymbol{k}'$–$\boldsymbol{j}'$ vector correlations. The results were interesting. The final state of the products shows strong directional preferences in the cold region and are less affected by the collinear approaching or departing geometries. With the continuous improvement of computing power, many new interesting phenomena have been gradually discovered in the in-depth study of LiH_2 reactive system [12–21] and some accurate PESs are constructed [17, 22], indicating the necessity of studying this chemical reaction.

The masses of electrons are much lighter than the masses of nuclei, thus the motion of electron moves so fast that can respond instantaneously to nuclear motion. Based on this, the Born–Oppenheimer (BO) approximation [23] was established, which proposed that the motion of electrons is separated from the nucleus in a molecular system. According to this approximation, the concept of adiabatic potential energy surface (PES) is proposed, greatly promoting the study of reaction dynamics. However, the limitations of BO approximation are recognized when a reaction process involves more than one adiabatic state [24, 25]. In some specific regions, the PES of the ground state is close to the excited states and the non-adiabatic couplings cannot be ignored [26]. There are two typical non-adiabatic effects [27, 28]. The PESs of two or more electronic states intersect each other in some regions, known as the conical intersection (CI) [29–32]. In recent years, the geometric phase (GP) effect [33–39], which is associated with the CI, has been proved to play an important role in the multi-state reaction dynamics. Xie *et al.* [40] studied the quantum interference in H + HD reaction. The interesting oscillation is observed, due to the strong quantum interference between direct abstraction and roaming insertion pathways around the CI. They mentioned the GP effect at the energy far below the CI can be probed by this oscillating pattern sensitively. Another kind of non-adiabatic effects is caused by the spin–orbit coupling (SOC) [41]. SOC affects the non-adiabatic reaction process by promoting the transition between states with different electron spins, and has been proved necessary in some chemical reactions [42–45]. These non-adiabatic effects have an obvious influence on the results of the reaction dynamics in many researches [46–49], which are sufficient to illustrate the necessity of taking the non-adiabatic effects into account in studying of some chemical reactions dynamics. However, the researches of non-adiabatic effects for LiH_2 system and its isotopic variants are not enough.

In this work, we focus on the impacts of the non-adiabatic effects on H + LiD reaction by comparing results between the adiabatic and non-adiabatic calculations. In 2016, our group developed a set of global diabatic PESs [50] (HYLC PESs) which include the ground state $1^2A'$ and the first excited state $2^2A'$. The *ab initio* points were calculated with the multi-reference configuration interaction method, and the diabatic energies were obtained based on the dipole moment operators. The non-adiabatic calculations are performed on the diabatic HYLC PESs directly. The adiabatic dynamical results are calculated on the ground-state adiabatic PES which is obtained by diagonalizing the diabatic potential energy matrix. The TDWP method is used to calculate the dynamical information of H + LiD reaction for both product channels in the collision energy range of 0.1–0.5 eV. The clearly physic pattern can be given by stereodynamical analysis to help understand the reaction progress, such as the kinetics of OH + HCl reaction [51], the foundation of origin of Anti–Arrhenius kinetics in OH + HBr reaction [52], the orientation dependent of OH + HBr reaction [53], and the non-adiabatic quenching of OH + H_2 system [54]. In our work, some stereodynamics are given to plaint a direct picture of reaction progress. This study can provide a basis for the subsequent study of the non-adiabatic dynamics of LiD depletion reactions. A brief description of the dynamical methodology is provided in Section 2. In Section 3, the relevant data are presented and the calculated results are discussed. The conclusions of this study are given in Section 4.

2 Theory

The TDWP method is proposed to investigate the adiabatic and non-adiabatic dynamics of H + LiD reaction. In this work, the improved L-shaped grid method developed by Buren *et al.* [55] is used, which is accurate enough in calculating the dynamics of atom–diatom reactive systems. This L-shaped grid method is an improvement of the conventional TDWP method. In the L-shaped grid method, the total scattering wave function is divided into two parts: the interaction region and the asymptotic region. According to the characteristics of the evolution of wave function, each region can be optimized

to describe the reaction dynamics efficiently and accurately.

Both the adiabatic and diabatic representations are defined in the reactant Jacobi coordinate (R, r, θ). For the adiabatic representation, the total Hamiltonian can be written as

$$\hat{H} = \hat{T} + \hat{V}, \tag{1}$$

where $\hat{T}$ is the kinetic energy operator and $\hat{V}$ is the reference potential energy operator. In the diabatic representation, the reaction contains two adiabatic states, and the total Hamiltonian can be written as

$$\hat{H} = \hat{T}\begin{pmatrix}1 & 0\\ 0 & 1\end{pmatrix} + \begin{pmatrix}V_{11} & V_{12}\\ V_{21} & V_{22}\end{pmatrix}. \tag{2}$$

The initial wave packet is set up with a Gaussian type function. The split-operator method is used in the propagation of wave packet [56]. The corresponding dynamical information can be extracted from the state-to-state S-matrix, written as

$$S^J_{v_f j_f l_f \leftarrow v_0 j_0 l_0}(E) = \frac{1}{\alpha(E)}\sqrt{\frac{k_f}{2\pi h^2 \mu_{R_f}}} h_{l_f}(k_f R_{f\infty})\langle \chi_{v_f j_f} | \Psi^+(E; R_{f\infty})\rangle, \tag{3}$$

where μ_{R_f} is the reduced mass at the product Jacobi coordinate, k_f is the wave vector in the product channel, h_{l_f} is the outgoing Ricatti-Hankel function, $R_{f\infty}$ is the product scattering coordinate in the product asymptote, $\alpha(E)$ is the amplitude of the initial wave function, $\Psi^+(E; R_{f\infty})$ means time-independent scattering wave function. The state-to-state integral cross sections (ICSs) are calculated by

$$\sigma_{v_f j_f \leftarrow v_0 j_0}(E) = \frac{\pi}{(2j_0+1)k^2_{v_0 j_0}} \sum_{l_0 l_f}\sum_J (2J+1)|S^J_{v_f j_f l_f \leftarrow v_0 j_0 l_0}(E)|^2 \tag{4}$$

and the state-to-state differential cross sections (DCSs) are computed by

$$\frac{\mathrm{d}\sigma_{v_f j_f \leftarrow v_0 j_0}(\vartheta, E)}{\mathrm{d}\Omega} = \frac{1}{(2j_0+1)}\sum_{K',K}\left|\frac{1}{2\mathrm{i}k^2_{v_0 j_0}}\sum_J (2J+1) d^J_{K'K}(\vartheta) S^J_{v_f j_f K' \leftarrow v_0 j_0 K}\right|^2, \tag{5}$$

where ϑ is the scattering angle, $k_{v_0 j_0}$ is the momentum in the entrance channel, $d^J_{K'K}(\vartheta)$ is the reduced rotation matrix.

In this work, all the Coriolis coupling effects are considered. To obtain fully converged results for H + LiD reaction, the initial wave packet is located at 15 a_0 in the L-shaped grid calculations. The maximum R coordinate used is 30 a_0 and 299 grids, and the maximum r coordinate used is 20 a_0 and 150 grids, which are precise enough for this study. The range of the total angular momentum quantum number is taken as $0 \le J \le 50$. The optimal parameters used in the L-shaped grid calculations are listed in Table 1.

3 Results and discussion

Based on HYLC PESs, both the adiabatic and non-adiabatic dynamical information of H + LiD reaction are calculated by the L-shaped grid method. In this reactive system, two product channels can be generated,

$$\mathrm{H}(^2\mathrm{S}) + \mathrm{LiD}(\mathrm{X}^1\Sigma^+) \rightarrow \mathrm{Li}(^2\mathrm{S}) + \mathrm{HD}(\mathrm{X}^1\Sigma^+_\mathrm{g}), \tag{R1}$$

$$\mathrm{H}(^2\mathrm{S}) + \mathrm{LiD}(\mathrm{X}^1\Sigma^+) \rightarrow \mathrm{D}(^2\mathrm{S}) + \mathrm{LiH}(\mathrm{X}^1\Sigma^+). \tag{R2}$$

The non-adiabatic effects are studied by comparing different results between the adiabatic and non-adiabatic calculations for both R1 and R2 channels. The characteristics of PESs are given to clarify the possible reaction mechanisms. For R1 channel, there is no barrier or well, which means that the direct reaction process dominates this channel. For R2 channel, there exist potential wells on the both V_{11} and V_{22} surfaces where complexes can be formed. In Fig. 1, the total ICSs of R1 and R2 channels are compared to understand the non-adiabatic effects of the title reaction in an intuitive way. The dash and solid lines represent the adiabatic and non-adiabatic results, respectively. The difference between the non-adiabatic and adiabatic results in R1 channel is more obvious than that in R2 channel. With the increase of collision energy, the discrepancies decrease in both channels. The reason

Table 1 Main parameters used in TDWP calculations for the H + LiD reaction. (Atomic units are used if not otherwise stated.)

Parameters	Values
R	$R \in [0.1, 30.0]$
	$N_R = 299$ (149 for interaction region)
r	$r \in [0.1, 20.0]$
	$N_r = 150$ (10 for asymptotic region)
θ	$N_\theta = 200$ (40 for asymptotic region)
Damping function for R	$R_a = 20.0$, $R_b = 30.0$, $C_R = 0.08$
Damping function for r	$r_a = 14.0$, $r_b = 20.0$, $C_r = 0.08$
Initial wave packet	$R_0 = 15.0$, $\delta = 0.5$ eV, $E_0 = 0.3$ eV
Total propagation time	40000(non-adiabatic), 30000(adiabatic)
Time step	$\Delta_t = 5$
Projection plane	$R_{f\infty} = 9.0$ for Li + HD,
	$R_{f\infty} = 13.0$ for D + LiH

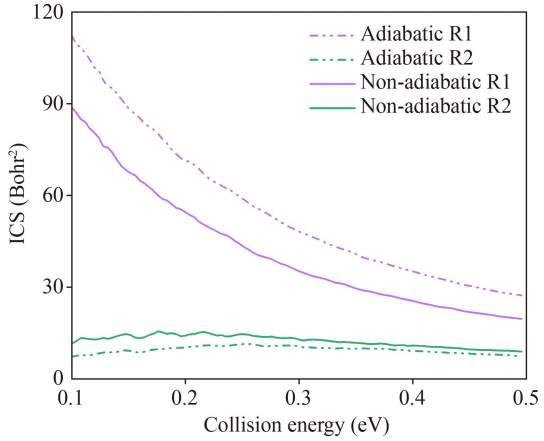

Fig. 1 Total ICS of different product channels for H + LiD reaction. R1 represents the depletion channel (H + LiD → Li(2s) + HD), and R2 represents the exchange channel (H + LiD → LiH + D).

of this phenomenon is that there are more paths without passing through the avoided crossing point to the product channel as the collision energy increases. The discrepancy becomes unobvious in R2 channel whereas it remains significant in R1 channel, indicating the important position of the non-adiabatic effects in R1 channel. The total ICS of R1 channel becomes smaller, while the total ICS of R2 channel becomes larger when the non-adiabatic coupling effects are taken into accounts, meaning that the different influences of the non-adiabatic effects for different product channels. To study this reaction in detail, we discuss different reaction channels respectively in the following.

R1 channel: $H(^2S)+LiD(X^1\Sigma^+)\rightarrow Li(^2S)+HD(X^1\Sigma_g^+)$

The vibrational state-resolved ICSs for R1 channel in the selected energy range are presented in Fig. 2 by the adiabatic (dash) and non-adiabatic (solid) calculations. The ICSs decrease with the increase of collision energy in both calculations. This variation is consistent with the exothermic reaction without barrier. The activity of the product is inhibited by the non-adiabatic effects at low vibrational states and slightly enhanced at high

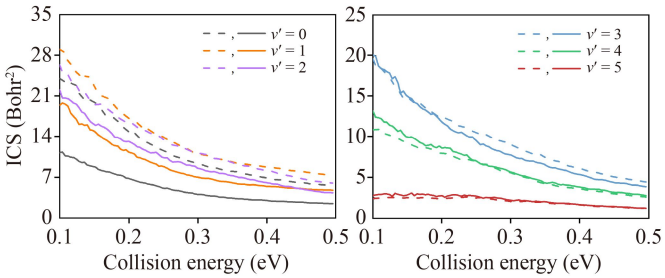

Fig. 2 The vibrationally state-resolved ICSs of the H + LiD → Li(2s) + HD reaction. Dash and solid lines are the adiabatic and non-adiabatic results, respectively.

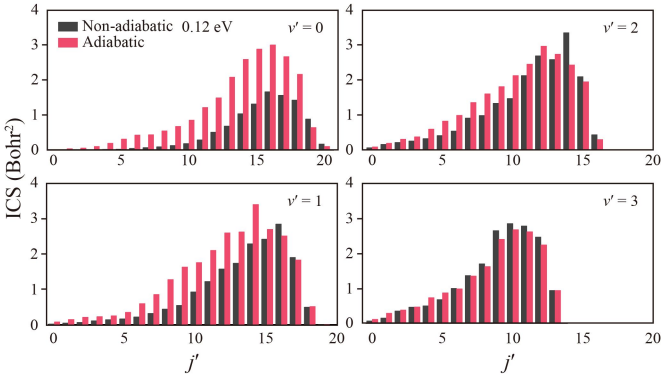

Fig. 3 Product ro-vibrational state distribution of H + LiD → Li(2s) + HD (ν', j') reaction at 0.12 eV collision energy.

vibrational states ($\nu' = 4$ and 5). The low vibrational-excited products have more prominent advantages than high vibrational-excited states products in the non-adiabatic calculations. However, the characteristics of ICSs are similar for products at different vibrational states in the adiabatic calculations. The largest populated vibrational state of products shifts from $\nu' = 1$ in the adiabatic calculations to $\nu' = 2$ in the non-adiabatic calculations. These changes mean that the non-adiabatic effects can promote the vibrational excitation of the product HD. The difference between the adiabatic and non-adiabatic results is obvious for the low vibrational state and gets smaller with the increase of the vibrational quantum number. For the vibrational quantum number larger than 3, there are some minor discrepancies caused by the non-adiabatic effects. For $\nu' = 5$, the curves almost coincide when the collision energy is higher than 0.3 eV.

Both the non-adiabatic and adiabatic ro-vibrational state product distributions of R1 channel at the collision energy of 0.12 and 0.48 eV are presented in Fig. 3 and Fig. 4, respectively. It can be seen from Fig. 3 that the available vibrational and rotational quantum numbers are barely affected by the non-adiabatic effects. At all

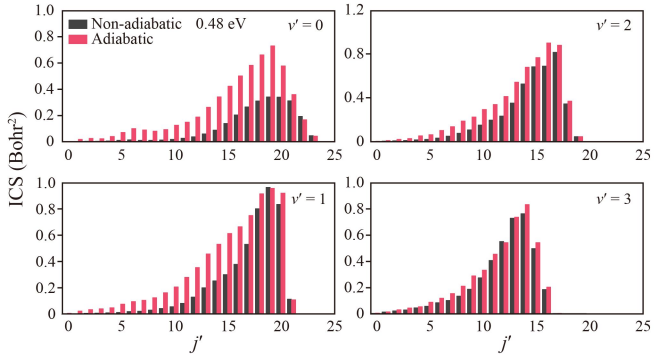

Fig. 4 Product ro-vibrational state distribution of H + LiD → Li(2s) + HD (ν', j') reaction at 0.48 eV collision energy.

the selected vibrational states, the products around the highest accessible rotational states are less influenced by the non-adiabatic effects than the products at low rotational states. For $\nu' = 0$, the reaction probability of the products is obviously suppressed by the non-adiabatic effects when the rotational quantum number is lower than 19. The inhibition of non-adiabatic effects gradually weakens, and this suppression is mainly reflected in the products at the intermediate accessible rotational states with the increase of the vibrational quantum number. Such similarity to the ro-vibrational state product distributions illustrates the unimportant effects of dominant reaction mechanism by the non-adiabatic couplings. In Fig. 4, the products prefer to distribute at the high rotational-excited states which is same with Fig. 3, meaning that the dominated reaction mechanism not changes. The product distribution at high vibrational states in both calculations are basically same, however the non-adiabatic effects play a key role in the product distribution at low vibrational states. With the increase of the vibrational quantum number, the influence of the non-adiabatic effects is gradually concentrated from most of the rotational states to the intermediate reachable rotational excited states. These features are consistent with the characteristics at 0.12 eV collision energy, revealing the influence of non-adiabatic effects is similar in the selected collision energy range.

The DCSs as a function of collision energy and scattering angle are plotted in Fig. 5. The products show mainly forward scattered bias in the selected collision energy range in both the adiabatic and non-adiabatic calculations. This characteristic is consistent with the stripping mechanism that product usually be excited to high rovibrational states and shows forward scattering [18, 57, 58]. Whereas, the product shows less polarized in the non-adiabatic calculations than in the adiabatic calculations. Backward scattering can be found when the collision energy is lower than 0.25 eV in the non-adiabatic calculations. These features are in line with the indirect mechanism which relates to the complex forming. Only one reaction mechanism dominates in this channel. The stereodynamical progress can be described as following: the stripping mechanism relates with the attractive PES. The center of mass of LiD molecule is close to Li atom, thus the receiving angle of D atom is much larger than that of Li atom, resulting in that H atom prefers to take the D atom away. A part of reaction exothermicity is translated into the translational energy of the HD molecule to keep it without changing the direction of motion in this channel. The vibrational excitation of products is related with the conservation of translational energy [20]. The low vibrational excited products are formed when the translational energy is less conserved. The reactivity of low vibrational excited product decreases especially at low collision energies, meaning the progress which is related with less conserved translational energy is affected by the non-adiabatic effects during H atom approaching LiD. The advantage of forward scattering diminishing may relate with this reason.

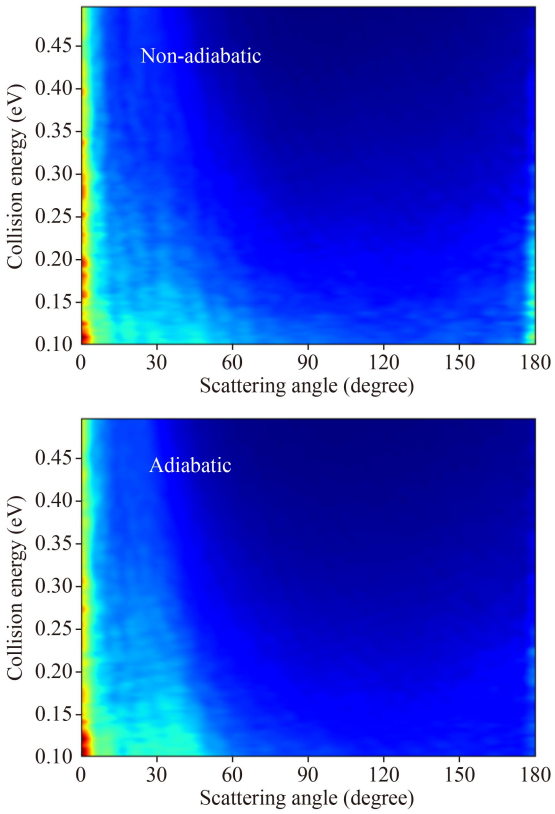

Fig. 5 Non-adiabatic and adiabatic DCSs of H + LiD → Li(2s) + HD reaction.

R2 channel: $H(^2S) + LiD(X^1\Sigma^+) \rightarrow D(^2S) + LiH(X^1\Sigma^+)$

For R2 channel, the vibrational state-resolved ICSs are presented in Fig. 6 by the adiabatic (dash) and non-adiabatic (solid) calculations. The highest vibrational state of products is at $\nu' = 2$. It is obviously less than the accessible vibrational state of R1 channel due to the large exothermic nature of it. The non-adiabatic couplings increase the reaction probability of this channel. There is an evident difference between the adiabatic and non-adiabatic results at the ground vibrational state especially when the collision energy is lower than 0.25 eV. The discrepancy decreases with the increase of collision energy. However, the ICS shows the opposite changes for the higher vibrational states ($\nu' = 1$ and 2). Oscillate structures are clearer in the non-adiabatic results especially at the ground vibrational state. This phenomenon means that the reaction progress becomes complex when the non-adiabatic effects are considered. To invest more details on the influence of the non-adiabatic effects, the product ro-vibrational state distribution of R2 channel is shown in Fig. 7. The non-adiabatic and

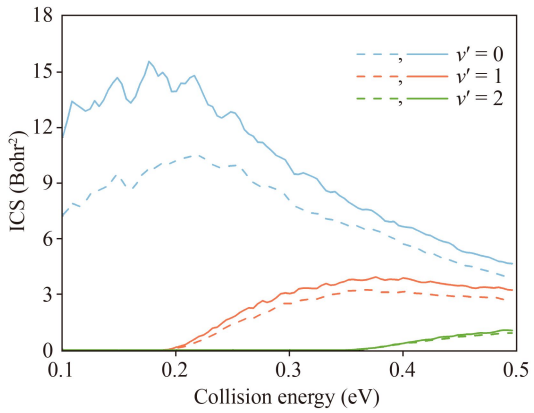

Fig. 6 The vibrational state-resolved ICSs of the exchange channel in the collision energy range from 0.1 to 0.5 eV. The solid and dash lines are non-adiabatic and adiabatic results, respectively.

adiabatic results of the product are represented by the solid and dash line of the same color, separately. The accessible number of ro-vibrational quantum numbers not changes, indicating that the rotational energy of products is barely influenced by the non-adiabatic effects. At the low collision energy, low vibrational-state products are evidently affected by the non-adiabatic effects. This influence gradually disappears as the increase of the rotational quantum number. In the adiabatic calculations, the distribution of the products is much flatter than that in the non-adiabatic calculations. The distribution consists with the characteristic of the rebound mechanism that the products population changes gently. While in the rebound mechanism, the product prefers relatively cold rotational distribution. This feature means the complex-forming also exists at this collision energy. In the non-adiabatic cases, the peak of the rotational states is close to the highest accessible rotational state, which means that the complex-forming mechanism has the dominated role at 0.12 eV collision energy. This difference indicates that the reaction mechanism is influenced by the non-adiabatic effects at this collision energy. The discrepancy of product distribution decreases between the adiabatic and non-adiabatic calculations with the increase of collision energy. The features of the complex-forming mechanism gradually diminish. At 0.48 eV collision energy, the distribution is flat in both calculations. This can be explained as the less effect of reaction mechanism by the non-adiabatic coupling. The reason for the different mechanisms at low collision energy is the formation of complex in the potential well when the non-adiabatic effects are considered.

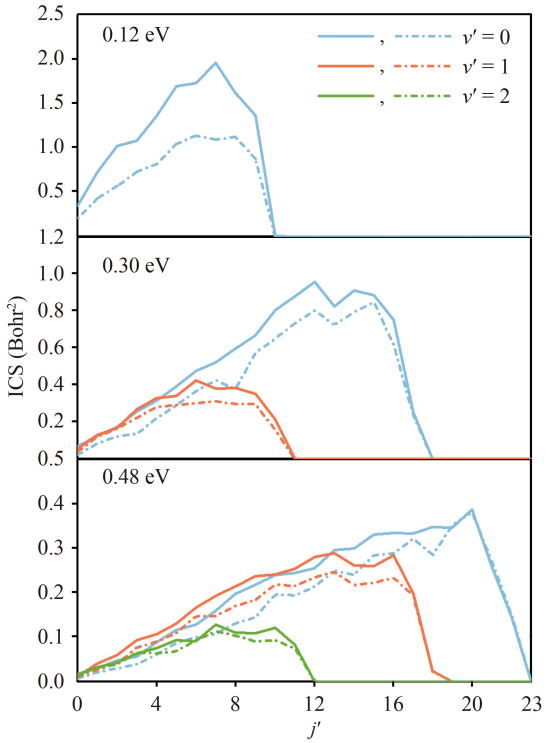

Fig. 7 Product ro-vibrational state distribution of the H + LiD → D + LiH reaction at three collision energies of 0.12, 0.30 and 0.48 eV. Solid and dash lines are the non-adiabatic and adiabatic results, respectively.

Based on these findings, the product angular distributions at three collision energies are also investigated. The DCSs as a function of scattering angle are painted in Figs. 8(a) and (b) corresponding to the non-adiabatic and adiabatic calculations, separately. At 0.12 eV collision energy, the product shows the forward-backward symmetric scattering in the non-adiabatic results. This phenomenon is in line with the characteristics of the complex-forming mechanism that the products are distributed near the polar angle and are symmetric. In the adiabatic calculations, both forward and backward exist. This phenomenon consists with our analysis in the product ro-vibrational distribution that both reaction mechanisms play roles in this channel. However, the backward scattering is stronger than the forward scattering, meaning the dominant role of rebound mechanism. At the higher energy (0.30 eV), the forward scattering

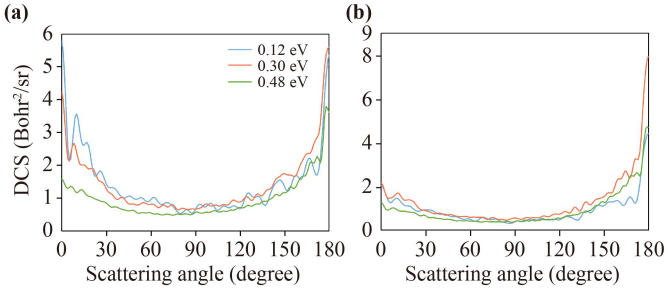

Fig. 8 Total DCSs of H + LiD → D + LiH reaction at three selected collision energies. **(a)** and **(b)** are the non-adiabatic and adiabatic results.

still exists in the non-adiabatic calculations, while the strict symmetry is not observed in the non-adiabatic calculations. At 0.48 eV collision energy, it has a similarly product angular distribution that backward scattering is predominant in both the non-adiabatic and adiabatic calculations. This product scattering means that the same reaction mechanism dominates both channels when the collision energy is 0.48 eV. The changes in product distribution may be caused by the shallow well in this channel, the complex-forming mechanism does not play an important role with the increase of collision energy. The DCS of the R2 channel is less polarized at low collision energy when the non-adiabatic effects are considered, due to the formation of the complex. As analyzed before, at 0.12 eV, the forward scattered products in non-adiabatic calculations are more obvious than in adiabatic calculations because of the different dominant mechanisms. The existence of the non-adiabatic couplings can cause a change in the reaction dominant mechanism. In the adiabatic calculations, the product distribution remains a backward scattered bias at all collision energies, which is related to the collinear collision rebound mechanism in the reaction paths. In the aspect of stereodynamics, on the way of H atom approaching LiD molecule, the process of movement is changed after considering the non-adiabatic effects, which affects the lifetime of complex in the shallow potential well of the reaction path. This change affects the distribution of the products and shows the different reaction mechanism at low collision energy. The reason of forward and backward symmetric product distribution is that the complex is formed in the potential well, and after a short time, it basically shows isotropy. With collision energy increasing, the effects of potential well become less obvious. At the time, H atom collides with LiD molecules without complex-forming mostly. LiD bond breaks and LiH molecule moves in the opposite direction. After collision, vibrational excitation of LiD reactant is produced, and the vibrational energy is transferred to LiH molecule. Compared with stripping mechanism, rebound mechanism corresponding to the small impact parameter collision, and product molecular rotational excitation is relatively cold.

4 Conclusion

In this work, both the adiabatic and non-adiabatic dynamical information of H + LiD reaction are calculated to study the non-adiabatic effects in this reaction. The reactivity of R1 reaction channel is inhibited while that of R2 channel is facilitated when the non-adiabatic couplings are considered. The non-adiabatic effects play an important role in promoting vibrational excitation for R1 channel. The rotational excitation of products at the ground vibrational state is suppressed by the non-adiabatic effects. For R1 channel, the stripping mechanism dominates the HD product channel in the selected collision energy range, and the main reaction mechanism is not significantly affected by the non-adiabatic effects. The complex formation shows as the less polarized product angular distribution in the non-adiabatic calculations. For R2 channel, compared with products at the vibrational-excited state, the non-adiabatic couplings obviously increase the formation of products at the vibrational ground-state, when the collision energy is lower than 0.24 eV. At relatively low collision energy, the complex forming mechanism dominates the reaction process when the non-adiabatic effects are considered, while the rebound mechanism becomes dominant with the increase of collision energy. In the adiabatic calculations, the rebound mechanism dominates R2 channel for all the selected collision energies. Above all, the presence of excited states has obvious effects on this reaction, especially in R1 channel. When considering the non-adiabatic effects, the results of the system should be closer to the actual situation, which provides a more comprehensive understanding of the depletion reaction of LiH/LiD molecules, and it is also hoped to provide a reference for the study of this system in astronomy.

Acknowledgements This work was supported by the National Natural Science Foundation of China (Grant No. 11774043).

Competing interests The authors declare no competing interests.

References

1. E. Bodo, F. A. Gianturco, and R. Martinazzo, The gas-phase lithium chemistry in the early universe: Elementary processes, interaction forces and quantum dynamics, *Phys. Rep.* 384(3), 85 (2003)
2. S. Lepp, P. Stancil, and A. Dalgarno, Atomic and molecular processes in the early universe, *J. Phys. At. Mol. Opt. Phys.* 35(10), 201 (2002)
3. Y. Zhang, N. Wang, Q. Li, L. Ou, J. Tian, M. Liu, K. Zhao, X. Wu, and Z. Li, Progress of quantum molecular dynamics model and its applications in heavy ion collisions, *Front. Phys.* 15(5), 54301 (2020)
4. Q. He, M. D. Reid, B. Opanchuk, R. Polkinghorne, L. E. Rosales-Zárate, and P. D. Drummond, Quantum dynamics in ultracold atomic physics, *Front. Phys.* 7(1), 16 (2012)
5. H. Zheng and Q. Gu, Dynamics of Bose–Einstein condensates in a one-dimensional optical lattice with double-well potential, *Front. Phys.* 8(4), 375 (2013)
6. J. Wu, R. Qi, A. Ji, and W. Liu, Quantum tunneling of ultracold atoms in optical traps, *Front. Phys.* 9(2), 137 (2014)
7. S. Lepp, and J. M. Shull, Molecules in the early universe, *Astrophys. J.* 280, 465 (1984)
8. N. J. Clarke, M. Sironi, M. Raimondi, S. Kumar, F. A. Gianturco, E. Buonomo, and D. L. Cooper, Classical and quantum dynamics on the collinear potential energy surface for the reaction of Li with H_2, *Chem. Phys.*

233(1), 9 (1998)
9. R. Padmanaban and S. Mahapatra, Time-dependent wave packet dynamics of the H + HLi reactive scattering, *J. Chem. Phys.* 117(14), 6469 (2002)
10. T. Roy, and S. Mahapatra, Quantum dynamics of H + LiH reaction and its isotopic variants, *J. Chem. Phys.* 136(17), 174313 (2012)
11. A. W. Huran, L. González-Sánchez, S. Gomez-Carrasco, and J. Aldegunde, A quantum mechanical study of the k–j and k'–j' vector correlations for the H + LiH → Li + H_2 reaction, *J. Phys. Chem. A* 121(8), 1535 (2017)
12. T. J. Martínez, *Ab initio* molecular dynamics around a conical intersection: Li(2p) + H_2, *Chem. Phys. Lett.* 272(3–4), 139 (1997)
13. L. G. Diniz, A. Alijah, and J. R. Mohallem, Benchmark linelists and radiative cooling functions for LiH isotopologues, *Astrophys. J. Suppl. Ser.* 235(2), 35 (2018)
14. J. Song and Z. Zhu, Dynamics studies of the Li(^{2}S) + $H_2(X^1\Sigma_g^+)$ → LiH($X^1\Sigma^+$) + H(^{2}S) reaction by time-dependent wave packet and quasi-classical trajectory methods, *Comput. Theor. Chem.* 1173, 112703 (2020)
15. D. He, J. Yuan, and M. Chen, Influence of rovibrational excitation on the non-diabatic state-to-state dynamics for the Li(2p) + H_2 → LiH + H reaction, *Sci. Rep.* 7(1), 3084 (2017)
16. J. Chen and K. Lin, Influence of vibrational excitation on the reaction Li(2^2P_J) + $H_2(\nu = 1)$ → LiH($X^1\Sigma^+$) + H, *J. Chem. Phys.* 119(17), 8785 (2003)
17. H. S. Lee, Y. S. Lee, and G. Jeung, Potential energy surfaces for LiH_2 and photochemical reactions Li^* + H_2 ↔ LiH + H, *J. Phys. Chem. A* 103(50), 11080 (1999)
18. X. He, H. Wu, P. Zhang, and Y. Zhang, Quantum state-to-state dynamics of the H + LiH → H_2 + Li reaction, *J. Phys. Chem. A* 119(33), 8912 (2015)
19. R. Padmanaban and S. Mahapatra, Resonances in three-dimensional H + HLi scattering: A time-dependent wave packet dynamical study, *J. Chem. Phys.* 120(4), 1746 (2004)
20. S. Gómez-Carrasco, L. González-Sánchez, N. Bulut, O. Roncero, L. Bañares, and J. F. Castillo, State-to-state quantum wave packet dynamics of the LiH + H reaction on two ab initio potential energy surfaces, *Astrophys. J.* 784(1), 55 (2014)
21. D. He, W. Li, and M. Wang, A study on the non-adiabatic dynamics of the Li(2p) + H_2 → Li(2s) + H_2 quenching reaction calculated by time-dependent wavepacket method, *Chem. Phys. Lett.* 780, 138910 (2021)
22. L. Fu, D. Wang, and X. Huang, Accurate potential energy surfaces for the first two lowest electronic states of the Li(2p) + H_2 reaction, *RSC Adv.* 8(28), 15595 (2018)
23. M. Born and W. Heisenberg, Zur quantentheorie der molekeln, in: Original Scientific Papers Wissenschaftliche Originalarbeiten, Springer, 1985, pp 216–246
24. D. V. Makhov, W. J. Glover, T. J. Martinez, and D. V. Shalashilin, *Ab initio* multiple cloning algorithm for quantum nonadiabatic molecular dynamics, *J. Chem. Phys.* 141(5), 054110 (2014)
25. B. F. Curchod, T. J. Penfold, U. Rothlisberger, and I. Tavernelli, Nonadiabatic *ab initio* molecular dynamics using linear-response time-dependent density functional theory, *Cent. Eur. J. Phys.* 11, 1059 (2013)
26. V. Betz and B. D. Goddard, Nonadiabatic transitions through tilted avoided crossings, *SIAM J. Sci. Comput.* 33(5), 2247 (2011)
27. Y. Guan, C. Xie, D. R. Yarkony, and H. Guo, High-fidelity first principles nonadiabaticity: Diabatization, analytic representation of global diabatic potential energy matrices, and quantum dynamics, *Phys. Chem. Chem. Phys.* 23(44), 24962 (2021)
28. F. Bernardi, M. Olivucci, and M. A. Robb, Potential energy surface crossings in organic photochemistry, *Chem. Soc. Rev.* 25(5), 321 (1996)
29. C. Xie, C. L. Malbon, H. Guo, and D. R. Yarkony, Up to a sign. The insidious effects of energetically inaccessible conical intersections on unimolecular reactions, *Acc. Chem. Res.* 52(2), 501 (2019)
30. H. Guo and D. R. Yarkony, Accurate nonadiabatic dynamics, *Phys. Chem. Chem. Phys.* 18(38), 26335 (2016)
31. C. Xie, D. R. Yarkony, and H. Guo, Nonadiabatic tunneling via conical intersections and the role of the geometric phase, *Phys. Rev. A* 95(2), 022104 (2017)
32. S. Mai, P. Marquetand, and L. González, A general method to describe intersystem crossing dynamics in trajectory surface hopping, *Int. J. Quantum Chem.* 115(18), 1215 (2015)
33. B. K. Kendrick, J. Hazra, and N. Balakrishnan, Geometric phase effects in the ultracold H + H_2 reaction, *J. Chem. Phys.* 145(16), 164303 (2016)
34. A. J. C. Varandas and H. G. Yu, Geometric phase effects on transition-state resonances and bound vibrational states of H_3 via a time-dependent wavepacket method, *J. Chem. Soc. Faraday Trans.* 93(5), 819 (1997)
35. H. Koizumi and S. Sugano, The geometric phase in two electronic level systems, *J. Chem. Phys.* 101(6), 4903 (1994)
36. J. C. Juanes-Marcos, S. C. Althorpe, and E. Wrede, Effect of the geometric phase on the dynamics of the hydrogen-exchange reaction, *J. Chem. Phys.* 126(4), 044317 (2007)
37. J. Huang and D. H. Zhang, An efficient way to incorporate the geometric phase in the time-dependent wave packet calculations in a diabatic representation, *J. Chem. Phys.* 153(14), 141102 (2020)
38. J. F. E. Croft, J. Hazra, N. Balakrishnan, and B. K. Kendrick, Symmetry and the geometric phase in ultracold hydrogen exchange reactions, *J. Chem. Phys.* 147(7), 074302 (2017)
39. D. Yuan, Y. Guan, W. Chen, H. Zhao, S. Yu, C. Luo, Y. Tan, T. Xie, X. Wang, Z. Sun, D. H. Zhang, and X. Yang, Observation of the geometric phase effect in the H + HD → H_2 + D reaction, *Science* 362(6420), 1289 (2018)
40. Y. Xie, H. Zhao, Y. Wang, Y. Huang, T. Wang, X. Xu, C. Xiao, Z. Sun, D. H. Zhang, and X. Yang, Quantum interference in H + HD → H_2 + D between direct abstraction and roaming insertion pathways, *Science* 368(6492), 767 (2020)
41. Y. Wang and D. R. Yarkony, Conical intersection

seams in spin–orbit coupled systems with an even number of electrons: A numerical study based on neural network fit surfaces, *J. Chem. Phys.* 155(17), 174115 (2021)
42. T. P. Rakitzis, Transition states and spin-orbit structure, *Science* 371(6532), 886 (2021)
43. W. Chen, R. Wang, D. Yuan, H. Zhao, C. Luo, Y. Tan, S. Li, D. H. Zhang, X. Wang, Z. Sun, and X. Yang, Quantum interference between spin-orbit split partial waves in the F + HD → HF + D reaction, *Science* 371(6532), 936 (2021)
44. J. Li, M. Sajjan, S. S. Kale, and S. Kais, Statistical correlation between quantum entanglement and spin–orbit coupling in crossed beam molecular dynamics, *Adv. Quantum Technol.* 4, 2100098 (2021)
45. T. Zimmermann and J. Vaníček, Evaluation of the importance of spin–orbit couplings in the nonadiabatic quantum dynamics with quantum fidelity and with its efficient "on-the-fly" ab initio semiclassical approximation, *J. Chem. Phys.* 137, 22A516 (2012)
46. Z. Yang, J. Yuan, S. Wang, and M. Chen, Global diabatic potential energy surfaces for the BeH_2^+ system and dynamics studies on the $Be^+(^2P) + H_2(X^1\Sigma_g^+) \rightarrow BeH^+(X^1\Sigma^+) + H(^2S)$ reaction, *RSC Advances* 8(40), 22823 (2018)
47. Z. Yang, Y. Mao, and M. Chen, Quantum dynamics studies of the significant intramolecular isotope effects on the nonadiabatic $Be^+(^2P)$ + HD → BeH^+/BeD^++ D /H reaction, *J. Phys. Chem. A* 125(1), 235 (2021)
48. Y. Mao, J. Yuan, Z. Yang, and M. Chen, Quantum dynamics studies of isotope effects in the $Mg^+(3p)$ + HD → MgH^+/MgD^+ + D/H insertion reaction, *Sci. Rep.* 10(1), 3410 (2020)
49. B. Buren, Y. Mao, Z. Yang, and M. Chen, Non-adiabatic couplings induced complex-forming mechanism in H + $MgH^+ \rightarrow Mg^+ + H_2$ reaction, *Chin. J. Chem. Phys.* 35(2), 345 (2022)
50. D. He, J. Yuan, H. Li, and M. Chen, Global diabatic potential energy surfaces and quantum dynamical studies for the $Li(2p) + H_2(X^1\Sigma_g^+) \rightarrow LiH(X^1\Sigma^+)$ + H reaction, *Sci. Rep.* 6, 25083 (2016)
51. N. D. Coutinho, F. O. Sanches-Neto, V. H. Carvalho-Silva, H. C. B. Oliveira, L. A. Ribeiro, and V. Aquilanti, Kinetics of the OH + HCl → H_2O + Cl reaction: Rate determining roles of stereodynamics and roaming and of quantum tunneling, *J. Comput. Chem.* 39(30), 2508 (2018)
52. N. D. Coutinho, V. H. Silva, H. C. de Oliveira, A. J. Camargo, K. C. Mundim, and V. Aquilanti, Stereodynamical origin of anti-arrhenius kinetics: negative activation energy and roaming for a four-atom reaction, *J. Phys. Chem. Lett.* 6(9), 1553 (2015)
53. P. Tsai, D. Che, M. Nakamura, K. Lin, and T. Kasai, Orientation dependence for Br formation in the reaction of oriented OH radical with HBr molecule, *Phys. Chem. Chem. Phys.* 13(4), 1419 (2011)
54. B. Zhao, S. Han, C. L. Malbon, U. Manthe, D. Yarkony, and H. Guo, Full-dimensional quantum stereodynamics of the nonadiabatic quenching of $OH(A^2\Sigma^+)$ by H_2, *Nat. Chem.* 13(9), 909 (2021)
55. B. Buren and M. Chen, Stereodynamics-controlled product branching in the nonadiabatic H + NaD → Na(3s, 3p) + HD reaction at low temperatures, *J. Phys. Chem. A* 126(16), 2453 (2022)
56. Z. Sun, S. Y. Lee, H. Guo, and D. H. Zhang, Comparison of second-order split operator and Chebyshev propagator in wave packet based state-to-state reactive scattering calculations, *J. Chem. Phys.* 130(17), 174102 (2009)
57. C. Yao, P. Zhang, Z. Duan, and G. Zhao, Influence of collision energy on the dynamics of the reaction $H(^2S)$ + $NH(X^3\Sigma^-) \rightarrow N(^4S) + H_2(X^1\Sigma_g^+)$ by the state-to-state quantum mechanical study, *Theor. Chem. Acc.* 133(6), 1489 (2014)
58. H. Song, S. Y. Lee, Z. Sun, and Y. Lu, Time-dependent wave packet state-to-state dynamics of H/D + HCl/DCl reactions, *J. Chem. Phys.* 138(5), 054305 (2013)